



1 A hydrogeomorphic dataset for characterizing catchment hydrological behavior 2 across the Tibetan Plateau

3 Yuhan Guo¹, Hongxing Zheng², Yuting Yang¹, Yanfang Sang³, Congcong Wen^{4,5}

4 ¹State Key Laboratory of Hydrosience and Engineering, Department of Hydraulic Engineering, Tsinghua University, Beijing,
5 100101, China

6 ²CSIRO Environment, Canberra, ACT 2601, Australia

7 ³Key Laboratory of Water Cycle and Related Land Surface Processes, Institute of Geographic Sciences and Natural Resources
8 Research, CAS, Beijing, 100101, China

9 ⁴NYUAD Center for Artificial Intelligence and Robotics, New York University Abu Dhabi, UAE

10 ⁵NYU Tandon School of Engineering, New York University, USA

11

12 *Correspondence to:* hongxing.zheng@csiro.au

13 Abstract

14 Hydrologic and geomorphic processes are intricately linked within the Earth system, jointly characterizing terrestrial
15 hydrological behaviors and biogeochemical cycles across diverse temporal and spatial scales. The Tibetan Plateau provides an
16 ideal setting for investigating the interactions between hydrological and geomorphic processes in a largely pristine natural
17 environment. Nonetheless, the interactions remain largely unknown due to challenging physical conditions and data limitations.
18 This study presents the inaugural version of a hydrogeomorphic dataset encompassing 18,440 catchments across the region.
19 The dataset comprises 18 hydrogeomorphic metrics, particularly along with the width function and width function-based
20 instantaneous unit hydrograph (WFIUH) of each catchment. We find that the peak flow of WFIUH is positively related to
21 slope and curvature but negatively related to catchment area, perimeter, length, and circularity. The relationships of time-to-
22 peak against the hydrogeomorphic metrics are similar to those of peak flow but in an opposite direction. Catchment
23 concentration time shows a positive relationship with catchment size but a strong negative correlation with catchment slope.
24 The validity of the derived WFIUH has been confirmed by its successful integration into an hourly hydrological model for
25 simulating flash flood events. Uncertainties in the WFIUH can be attributed to the resolution of DEM and the methods
26 employed for calculating flow velocity. The dataset is publicly available via the Zenodo portal:
27 <https://doi.org/10.5281/zenodo.8280786> (Guo and Zheng, 2023). It can contribute to advancing our understanding of
28 catchment hydrological behaviors in the Tibetan Plateau and hence improving water resources management and disaster
29 mitigation in the region and its downstream.



30 **1 Introduction**

31 Hydrologic and geomorphic processes are intricately linked within the Earth system, jointly characterizing terrestrial
32 hydrological processes and biogeochemical cycles across diverse temporal and spatial scales. The interactions between these
33 processes play a critical role in governing water flow, shaping landforms, and influencing sediment and nutrient transportation
34 within ecosystems (Babar, 2005; Scheidegger, 1973; Sidle and Onda, 2004). The exploration of the interactions can be traced
35 back to Horton's foundational contributions (Horton, 1945) and the classical works of Strahler (1957), Kirkby (1976) and
36 Rodríguez-Iturbe and Valdés (1979). Since then, extensive endeavors have been undertaken in hydrology and geomorphology
37 to investigate the hydrologic behavior of a catchment in response to its geomorphic attributes (Jenson, 1991).

38 Hydrogeomorphologic data consisting of various geomorphic attributes (e.g., slope, elevation, curvature, and catchment
39 shape attributes) has demonstrated value in predicting hydrological behavior for ungauged basins (Esper Angillieri, 2008),
40 mapping flood-prone zones (Lindersson et al., 2021) and determining the groundwater potential zones. On top of the
41 morphologic or topographic metrics describing catchment properties, the geomorphologic instantaneous unit hydrograph
42 (GIUH) introduced by Rodríguez-Iturbe and Valdes (1979) is of utmost interest for hydrologists to derive hydrograph in the
43 absence of hydrologic data (Bhaskar et al., 1997; Jain et al., 2000; Nasri et al., 2004; Nowicka and Soczynska, 1989; Kumar
44 et al., 2007). The concept of GIUH was extended by Gupta et al. (1980) to theoretically deduce the unit hydrograph based on
45 geomorphology, topographic parameters, and hydrographic parameters. The GIUH assumes that the probability distribution
46 of the water droplet travel time is exponential, which however lacks practical physical meaning (Gupta and Waymire, 1983;
47 Kirshen and Bras, 1983; Rinaldo et al., 1991). The assumption is arguable and it is also challenging to determine flow velocity
48 while deriving GIUH (Rodríguez-Iturbe and Valdes, 1979; Troutman and Karlinger, 1985). An alternative geomorphology-
49 based unit hydrograph is based on the geomorphic width function (Kirkby, 1976). The width function is commonly considered
50 as one of the most important geomorphologic and hydrologic features quantifying the influence of the river network on
51 catchment hydrologic processes (Mesa and Mifflin, 1986; Naden, 1992), which determines the shape of the instantaneous unit
52 hydrograph (Botter and Rinaldo, 2003). Franchini and O'connell (1996) compared WFIUH against GIUH and suggested that
53 WFIUH is more physically consistent and more practical.

54 The Tibetan Plateau is known as the water tower of Asia, supplying water to almost 2 billion people (Yao et al., 2012; Li
55 et al., 2022; Mtamba et al., 2015). Hydrogeomorphic characteristics of catchments within the Tibetan Plateau are unique and
56 with little human intervention (Yao et al., 2022; Mölg et al., 2014). The geographical uniqueness of the Tibetan Plateau
57 provides ideal opportunities to explore the interactions between hydrologic and geomorphic processes. However,
58 hydrogeomorphic data of catchments across the Tibetan Plateau are still limited for a systematic investigation of the
59 hydrogeomorphic process in the region. Particularly, the Tibetan Plateau is experiencing more extreme precipitation events
60 and floods (Ge et al., 2019; Yang et al., 2022), which makes it imperative to develop a comprehensive hydrogeomorphic
61 dataset to inform flood modeling and adaptive watershed management.

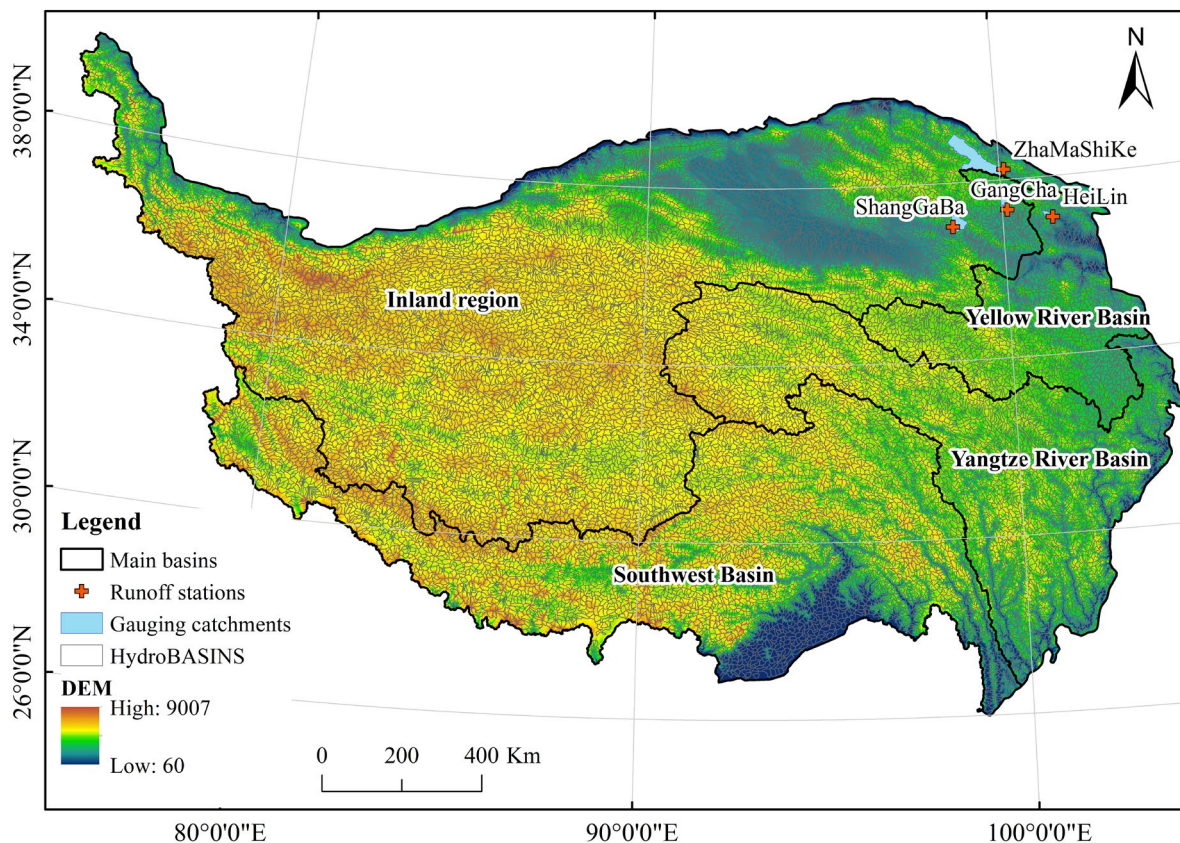


62 This research aims to provide an inaugural version of the hydrogeomorphic dataset for catchments over the Tibetan
63 Plateau. The dataset includes 18 hydrogeomorphic measurements of 18440 catchments within the plateau, which are derived
64 from a high-resolution digital elevation model (DEM) or compiled from existing products. Most importantly and uniquely, the
65 research provides the first dataset of WFIUH for each catchment, which can be used to investigate the spatial heterogeneity of
66 hydrological behavior across the Tibetan Plateau. The derived WFIUH are tested and validated as applied to flood modeling
67 for gauged catchments. This dataset is expected to contribute to a better understanding of hydrogeomorphic processes and to
68 facilitate hydrological modeling of catchments across the Tibetan Plateau.

69 2 Study area and data

70 The Tibetan Plateau (TP) is situated between 26°00 to 40°N and 73° to 105°E and has a mean elevation of more than
71 4500 meters, occupying about 2.5×10^6 km². TP is the highest and most extensive highland in the world. In addition to having
72 the largest cryospheric extent outside the polar region, the TP also serves as the source region for all major rivers in Asia.
73 Consequently, it has been widely acknowledged as the driving force behind both regional and global environmental change
74 (Kang et al., 2010). The Mekong River, the Yellow River, the Yangtze River, the Yarlung Tsampo (Brahmaputra), the Indus
75 and the Karnali all originate on the Tibetan plateau and support hundreds of millions of people downstream. Due to the harsh
76 and complex natural environment, the Tibetan Plateau is a typical ungauged area in China. Within the boundary of China, the
77 Tibetan Plateau can be roughly divided into several basins, namely the Inland region basin, the Yellow River basin, the Yangtze
78 River basin, and the Southwest basin (Figure 1).

79 In this study, the hydrogeomorphic dataset we developed covers 18440 catchments across the Tibetan Plateau. The
80 boundaries of the catchments are determined according to the HydroBASINS dataset, where the 12th level catchments are
81 considered (<https://www.hydrosheds.org/products/hydrobasins>). In deriving the width function for each catchment, the flow
82 direction raster map from HydroSHEDS (<https://www.hydrosheds.org/hydrosheds-core-downloads>) is also used, which based
83 on DEM from NASA's Shuttle Radar Topography Mission (SRTM) with spatial resolution around 90m (Lehner et al., 2008).
84 Land cover data product FROM-GLC (Finer Resolution Observation and Monitoring-Global Land Cover) released by
85 Peng Gong et al. (2019) is used in this study to estimate the Manning coefficient in calculating flow velocity. The spatial
86 resolution of the land cover data is 10m. It is resampled by the bilinear approach to be consistent with the flow direction
87 map. For hydrological modeling validity, hourly rainfall and streamflow data of 4 hydrological stations are obtained from
88 China's Annual Hydrological Report. Boundaries of the 18440 catchments and locations of the hydrological stations are shown
89 in Figure 1.

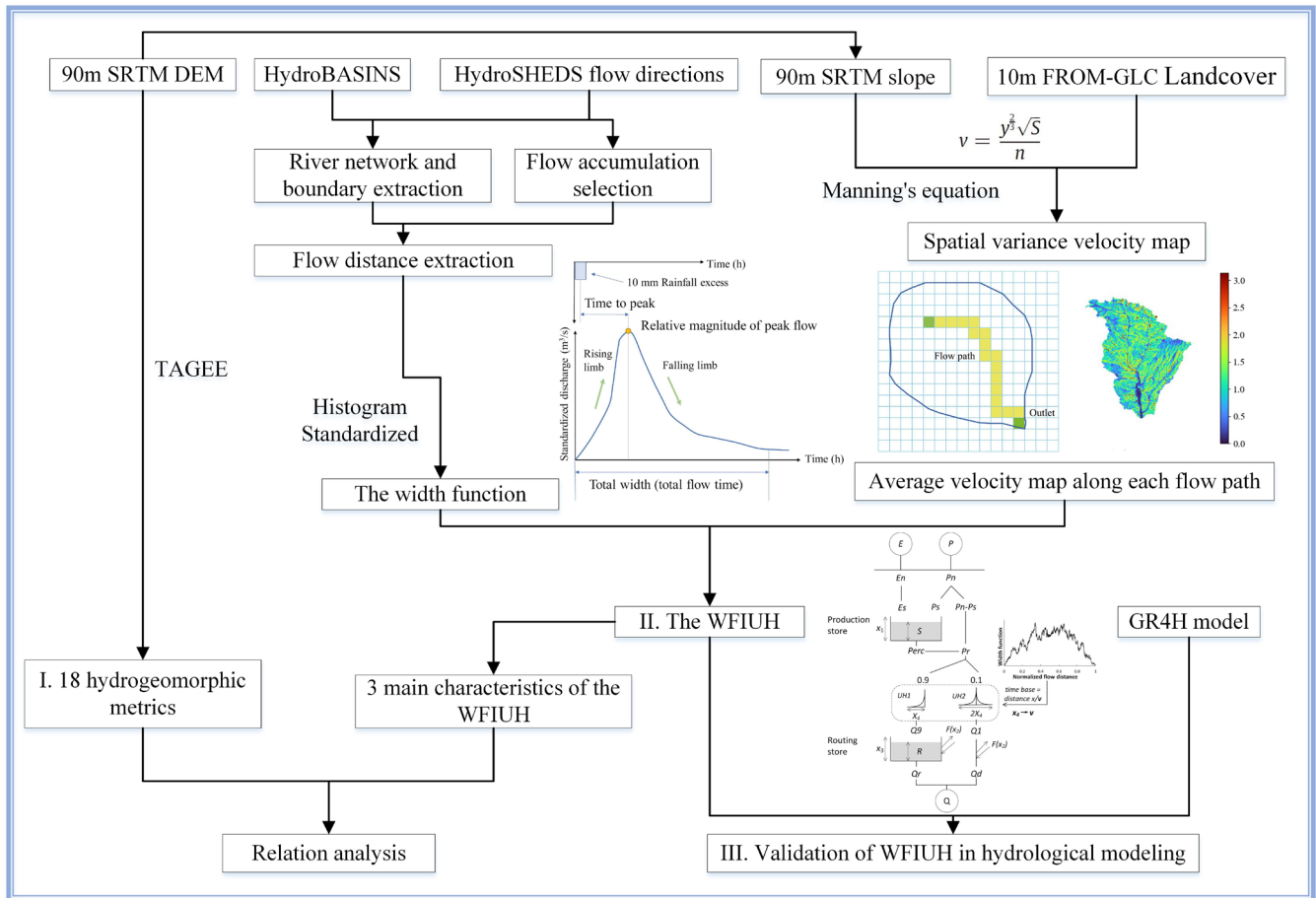


90
91 **Figure 1** Elevation and boundaries of 18440 catchments across the Tibetan Plateau

92 **3 Methods**

93 The overall framework for producing the hydrogeomorphic dataset for catchments over the Tibetan Plateau is shown in
94 Figure 2. The framework mainly consists of three procedures, i.e., extracting critical hydrogeomorphic metrics from DEM or
95 existing data products, deriving width function for catchments based on terrain analysis, and generating WFIUH for all
96 catchments. The derived WFIUH is then tested by incorporating it into a hydrological model to simulate hydrological processes
97 at a catchment scale.

98



99
 100 **Figure 2 Framework of developing catchment-scale hydrogeomorphic dataset of the Tibetan Plateau**

101 **3.1 Catchment-scale hydrogeomorphic metrics**

102 In this dataset, 18 hydrogeomorphic metrics at a catchment scale are retrieved from DEM or compiled from existing
 103 datasets. The hydrogeomorphic metrics are closely related to hydrologic and geomorphic processes for the catchments,
 104 including area, consisting of area, the longitude of centroid, latitude of centroid, mean elevation, slope, aspect, northness,
 105 eastness, perimeter, catchment length, catchment width, elongation, circularity index, form factor, shape index, Gaussian
 106 curvature, hillshade, horizontal curvature and vertical curvature. Definitions of each metric are shown in Table 1.

107 Several topographic and geomorphic attributes are gained from a package called Terrain Analysis in Google Earth Engine
 108 (TAGEE) (Safanelli et al., 2020) using Google Earth Engine platforms. The curvature shows the complexity of the undulation
 109 of the ground and it is a quantitative measure of curvature degree and change-point on the terrain surface. The horizontal
 110 curvature indicates the degree of curvature and change of the surface along the horizontal direction, which could affect the
 111 convergence and dispersion of water flow. The vertical curvature is the degree of elevation change along the maximum slope
 112 of the ground slope, which could affect the speed of water flow, resulting in different erosion or accumulation rates. Mean



113 curvature and the Gaussian curvature both characterize the comprehensive curvature features. According to Safanelli et al.
 114 (2020), Northness and Eastness can be derived from the aspect. The aspect and derived products, such as Northness and
 115 Eastness attributes, can be linked to the potential solar irradiation on terrain. Mathematical expressions of these metrics listed
 116 in Table 1 can be referred to Florinsky (2016). It is worth noting that the shape index (SI) is a continuous numerical form of
 117 Gaussian landform classification proposed by Koenderink and Van Doorn (1992). The range of the shape index is -1 to 1.
 118 When the value is negative, the surface is concave, and if the value is positive, the surface is convex. When the absolute value
 119 of the shape index is within 0.5-1.0, the surface is elliptical. When the absolute value of the shape index is within 0-0.5, the
 120 surface is hyperbolic. The shape index expression is as follows:

$$121 \quad SI = \frac{2}{\pi} \arctan \frac{H}{\sqrt{H^2 - K}} \quad (1)$$

122 In the formula, H and K are parameters used to characterize the shape of the surface (such as ridge or valley, convex or
 123 concave). For illumination of the datasets, the expressions of circularity index (CI), form factor (Rf), elongation ratio (Re) and
 124 are presented respectively herein:

$$125 \quad CI = \frac{A_{\text{catchment}}}{A_{\text{circle}}} \quad (2)$$

$$126 \quad R_f = \frac{A_{\text{catchment}}}{L_{\text{catchment}}^2} \quad (3)$$

$$127 \quad R_e = \frac{L_{\text{circle}}}{L_{\text{catchment}}} \quad (4)$$

128 where, $A_{\text{catchment}}$, $L_{\text{catchment}}$ are the area and length of a catchment. A_{circle} is the area of a circle whose perimeter equals
 129 the watershed's perimeter. L_{circle} is the diameter of a circle that equals the catchment area. The circularity index represents
 130 the ratio of the catchment area to the area of a circle with an equivalent perimeter. It ranges between 0 and 1. The catchment
 131 is closer to a circular shape for a higher CI value. The Form factor is the ratio of catchment area to squared catchment length.
 132 A higher Rf indicates a closer fan-shaped catchment. The Elongation ratio is the ratio of L_{circle} to catchment length. A smaller
 133 value of Re reflects a more elongated catchment.

134 Metrics such as area, perimeter, catchment length, catchment width, elongation ratio, circularity index, and form factor are
 135 retrieved from HydroBASINS sub-catchment shapes. The elevation and slope metrics are derived from SRTM DEM with a
 136 spatial resolution of around 90m. Before retrieving the metrics for the Tibetan Plateau domain, all the maps have been
 137 reprojected to the same coordination system.

138 **Table 1 Descriptions of 18 hydrogeomorphic metrics provided in TPHGD dataset**

Metrics	Descriptions	Units
Area	Area of catchment	km ²
Perimeter	Perimeter of catchment	km
Catchment length	Straight distance from the outlet to the farthest point in a catchment	km



Catchment width	The narrowest distance perpendicular to the line between the outlet and the farthest point	km
Elevation	The mean elevation of catchment	meter
Slope	Mean slope of the catchment	degree
Aspect	Compass direction	degree
Northness	Degree to north	N/A
Eastness	Degree to east	N/A
Circularity index	see formula 2	N/A
Form factor	see formula 3	N/A
Elongation ratio	see formula 4	N/A
Shape index	Continuous form of Gaussian landform classification, see formula 1	N/A
Hillshade	Brightness of illuminated terrain	N/A
Horizontal curvature	Curvature tangent to the contour line	meter
Vertical curvature	Curvature tangent to slope line	meter
Gaussian curvature	Product of maximal and minimal curvatures	meter
Mean curvature	Mean of horizontal and vertical curvatures	meter

139

140 3.2 Width function from DEM

141 The width function (WF) of a catchment is more informative than a single hydrogeomorphic metric in reflecting runoff
 142 response to catchment landforms. The width function is defined as the probability measure at a given distance x to the outlet
 143 of the i_{th} link measured along with the river network (Rinaldo et al., 1995). With the assumption that every water drop in the
 144 channel network travels to the outlet at the same velocity, mathematically, the width function $W(x)$ is expressed:

$$145 \quad W(x) = \sum_{i=1}^n b(x; x_i^u, x_i^d) \quad (5)$$

146 where n is the number of links in the network, x_i^u and x_i^d are the distances of the upstream and downstream ends of link i from
 147 the outlet, and the function $b(x)$ is expressed as:

$$148 \quad b(x; x_i^u, x_i^d) = \begin{cases} 1, & x_i^d \leq x < x_i^u \\ 0, & \text{otherwise} \end{cases} \quad (6)$$

149 Integrated along the longest flow path, the relationship between the catchment area and the width function can then be
 150 expressed as (Moussa, 2008):

$$151 \quad Area = \int_0^{L_{max}} W(x) dx \quad (7)$$

152 Therefore, for comparison among different catchments, the width function can be normalized as:

$$153 \quad W'(x^*) = W(x)/Area, \text{ with } x^* = x/L_{max} \quad (8)$$

154 In this study, we develop the width function for each catchment based on the flow direction map from HydroSHEDS by
 155 using the *pysheds* package in Python (<https://github.com/mdbartos/pysheds>). Given the flow direction map, catchment
 156 delineation and river network extraction proceeded after the implementation of flow accumulation. The threshold of flow
 157 accumulation is set to be the 96th percentile of the total accumulation as an easy and efficient way compared with other more



158 complex methods (Passalacqua et al., 2010). Based on the derived river network, the flow distance of each DEM grid is
159 computed and the width function is estimated as the histogram of the catchment area (represented by the number of grids)
160 against flow distance.

161 3.3 Width function-based instantaneous unit hydrograph

162 The width function is closely related to the development of a geomorphic instantaneous unit hydrograph (Singh et al.,
163 2014). The WF-based IUH (i.e., WFIUH) is the combination of the WF with any possible linear routing scheme. If only river
164 network routing is taken into account, the convection-diffusion equation can be applied to calculate the WFIUH after stream
165 network ordering (Franchini and Oconnell, 1996). The expression form of WFIUH becomes the following form:

$$166 \quad WFIUH(t) = \int_0^{L_{max}} f_x(t)W(x)dx \quad (9)$$

167 where, $f_x(t)$ represents the flow time distribution at the distance x along the river network in a watershed and $W(x)$ is the
168 width function. L_{max} is the largest length of the stream network.

169 Equation 9 ignores hillslope routing within a catchment. The hillslope routing however could be a critical process in
170 determining runoff response to rainfall and shaping the IUH (Saco and Kumar, 2004). With the consideration of the effects of
171 hillslope routing, it is proposed to combine the spatial distribution of flow velocity and the width function to derive WFIUH
172 (Grimaldi et al. (2010), which is adopted in this study. Four approaches are commonly used to calculate flow velocity (Grimaldi
173 et al., 2010), including Darcy–Weisbach’s formula (Katz et al., 1995), Manning’s formula, the Soil Conservation Service (SCS)
174 formula (Haan et al., 1994), and the uniform flow formula (Maidment et al. (1996). Making use of a remotely sensed land
175 cover dataset, we herein adopt Manning’s formula in our calculation, which is expressed as:

$$176 \quad v = \frac{y^{\frac{2}{3}}\sqrt{S}}{n} \quad (10)$$

177 where, n is Manning’s roughness coefficient that is related to the land cover type of catchments, and its unit is $m^{-\frac{1}{3}}s$.

178 To calculate the velocity, as shown in Figure 2, a spatial map of the slope for each catchment is produced based on DEM
179 from SRTM. The 10m FROM-GLC landcover data is then resampled to 90m resolution to match with that of DEM. Manning’s
180 roughness n for each 90m grid was assigned according to the look-up table of land cover type against roughness (Table S1 in
181 Supplementary).

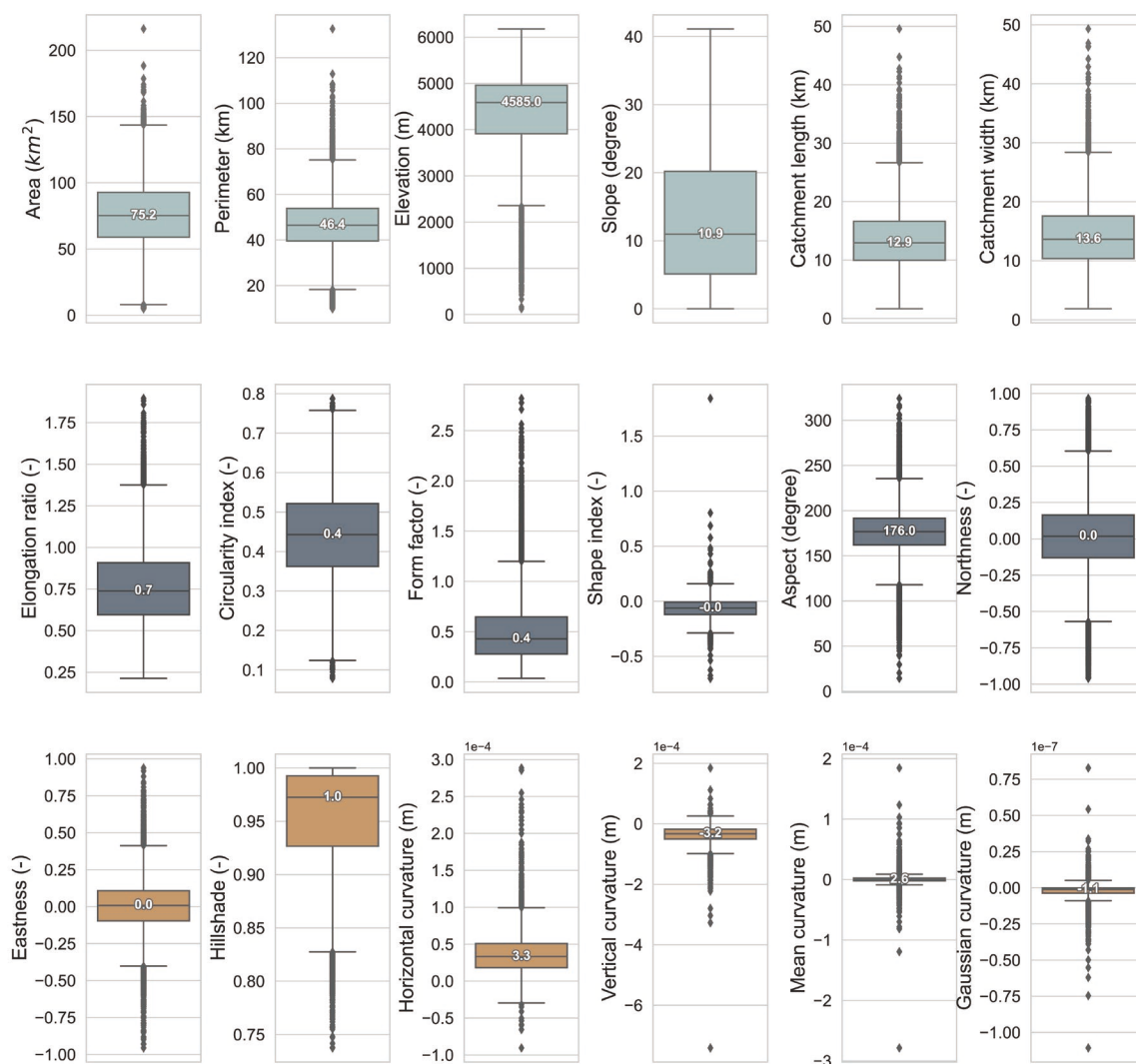
182 4 Results

183 4.1 Spatial distribution of hydrogeomorphic characteristics

184 Eighteen hydrogeomorphic metrics of 18440 catchments across the Tibetan Plateau are provided in our dataset (TPHGD).
185 Metrics of a small portion of catchments (<1%) are missing due to spatial mismatch or data quality. Figure 3 presents a
186 statistical summary of the metrics, while Figure 4 shows spatial patterns of the metrics across the Tibetan Plateau. As shown



187 in Figure 3, the area of the 18440 catchments ranges between 4.8 km² and 216 km², with perimeter that varies from 9.8 km to
 188 132.7 km and catchment mean elevation between 123.8m to 6180.9m. Most of the catchments are located between 2200m and
 189 6100m. Catchments with higher elevations are in the western and central parts of the TP. Catchments in the western and
 190 southeast TP are steeper than other catchments in the TP. Catchment length and width are similar in their statistical distribution
 191 (Figure 3), both largely between 1-30km.

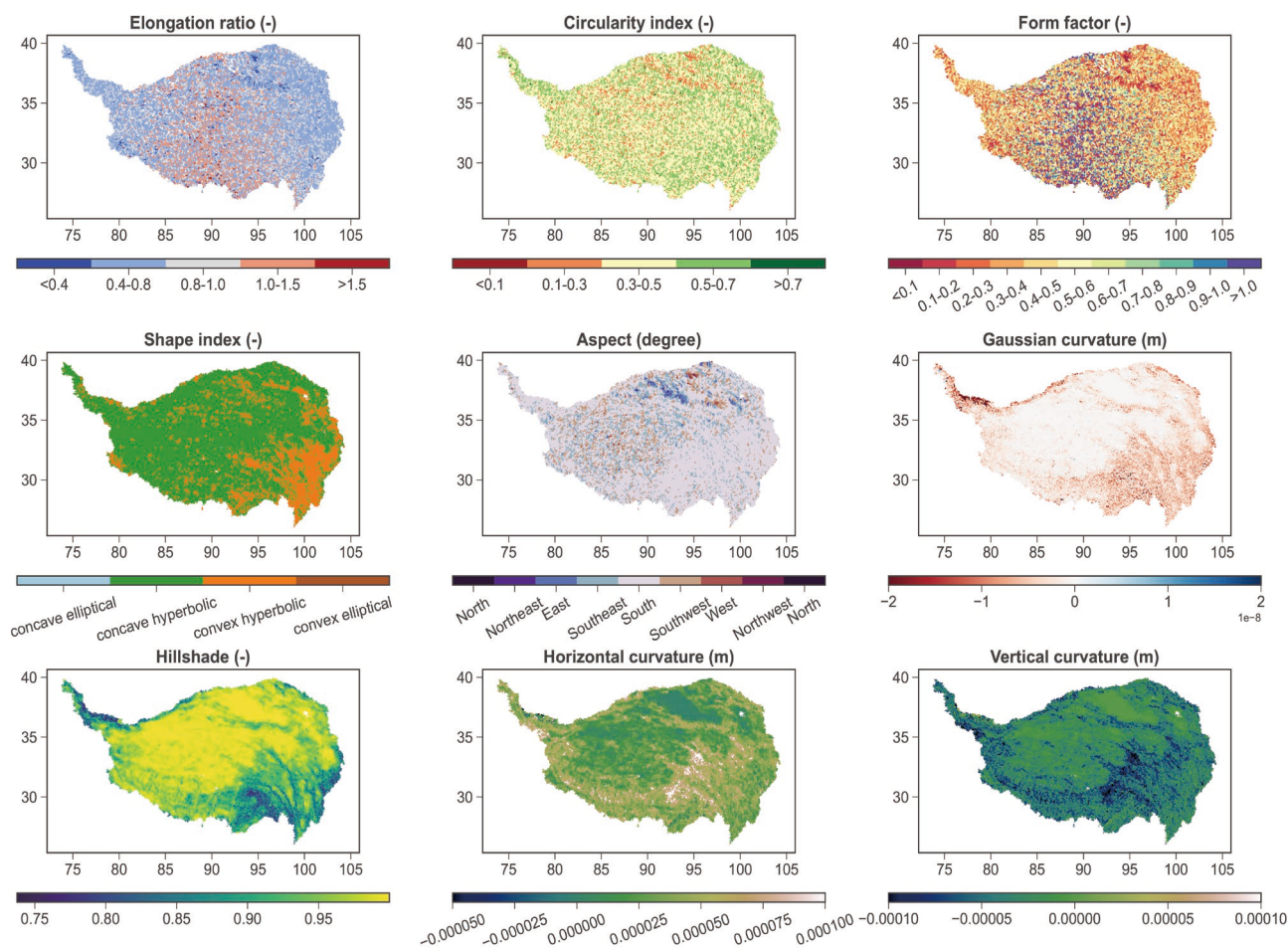


192
 193 **Figure 3 Statistical summaries of 18 hydrogeomorphic metrics for 18440 catchments across the Tibetan Plateau.**

194 Ranges of the elongation ratio, circularity index, and form factor of the catchments are 0.2-1.9, 0.08-0.79, and 0.04-2.82
 195 respectively. Around three-quarters of the catchments have an elongation ratio lower than 1, which means the majority of
 196 catchments tend to be elongated. Catchments in central TP are more elongated ($Re > 1.0$) and are with a pinnate river network

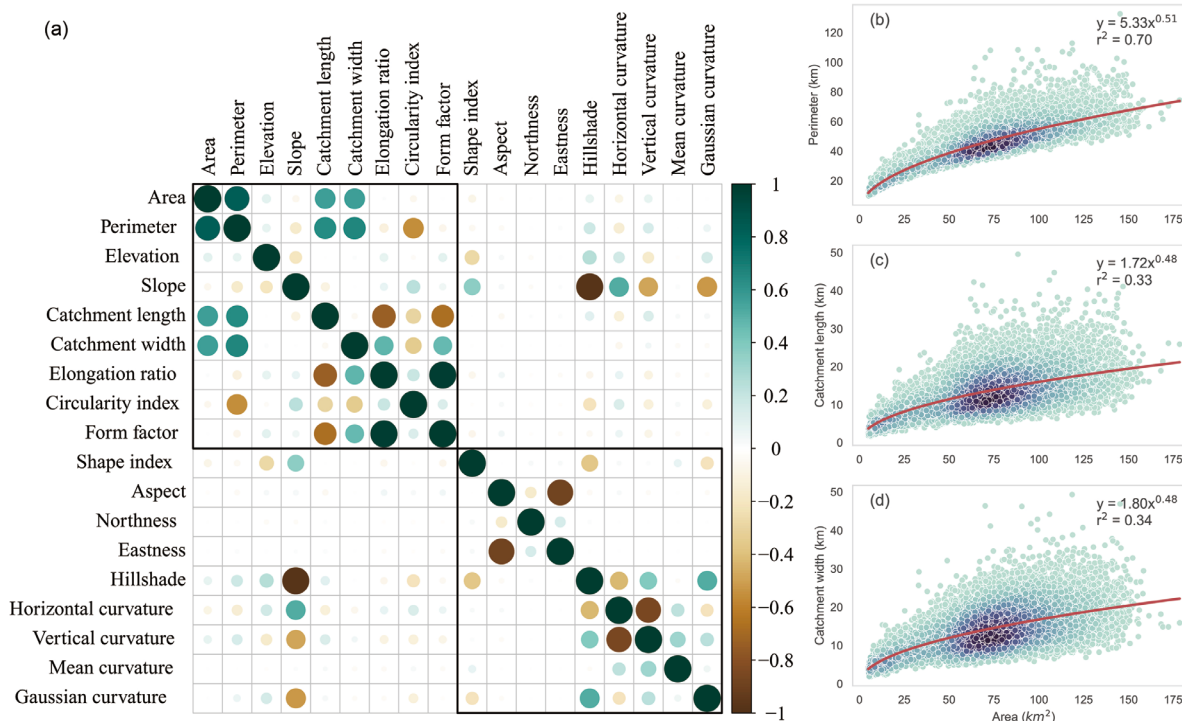


197 ($R_f > 1.0$). Catchments located in western and eastern TP are less elongated and more fan-shaped (Figure 4). Most catchments
198 show concave hyperbolic land surface, with a shape index between -0.5 and 0, except for catchments located in the southeast
199 TP. Most catchment aspects are between 150 and 200 degrees with their northness and eastness ranging between -0.25-0.25
200 and -0.5-0.5 respectively. This reveals that most catchments in TP face southwest, south, or southeast. Hillshade of most
201 catchments is above 0.9 (Figure 3). Catchments in southeast TP have lower hillshade, suggesting that they are in the alpine
202 and valley areas with a higher shading effect. The curvature of a catchment affects the movement of water, sediment and
203 biogeochemical matters. In addition to the horizontal and vertical curvatures, the Gaussian and mean curvatures for each
204 catchment are recorded in our dataset as well. The median horizontal and vertical curvatures of all the TP catchments are
205 around 0.33×10^{-3} m and -0.32×10^{-3} m respectively. Medians of mean and Gaussian curvature are 0.26×10^{-3} m and -0.11×10^{-6}
206 m respectively. It is worth noting that the curvature metrics in our dataset represent that at a catchment scale, which are averages
207 of each grid cell within the catchment. Hence, catchments with less curvature suggest a greater extent of flat or plain terrain
208 within the catchment.
209



210
 211 **Figure 4 Spatial patterns of hydrogeomorphic metrics across the Tibet Plateau**

212 Figure 5 shows correlations among the 18 metrics. Catchment area (A_c) is found significantly correlated with catchment
 213 length (L_c), width (L_w), and perimeter (P_c), and could be represented by the power law (Figure 5(b), (c), (d)). The relationship
 214 between A_c and L_c largely follows Hack's law (Rigon et al., 1996; Sassolas-Serrayet et al., 2018), which suggests a power
 215 law between the length of the river channel and drainage area. The catchment perimeter is negatively correlated with the
 216 circularity index (with a correlation coefficient $r = -0.55$). Elongation ratio, circularity index, and form factor are highly related
 217 to catchment length, catchment width, and perimeter as can be expected according to Eqs.2-4. The form factor and the
 218 elongation ratio are highly related ($r = 0.98$). This may indicate that the elongation ratio and form index represent similar shape
 219 information of a catchment. The slope of the catchments is correlated negatively with hillshade ($r = -0.97$), vertical curvature
 220 ($r = -0.49$) and Gaussian curvature ($r = -0.53$), but positively with shape index ($r = 0.36$) and horizontal curvature ($r = 0.52$). There
 221 is no significant correlation between catchment slope and elevation with a correlation coefficient of no more than ± 0.3 .



222

223 **Figure 5 Correlation between the 18 hydrogeomorphic metrics (left) and relationships between catchment area against catchment**
 224 **length, width and perimeter (right).**

225 **4.2 Classification of catchment's width function**

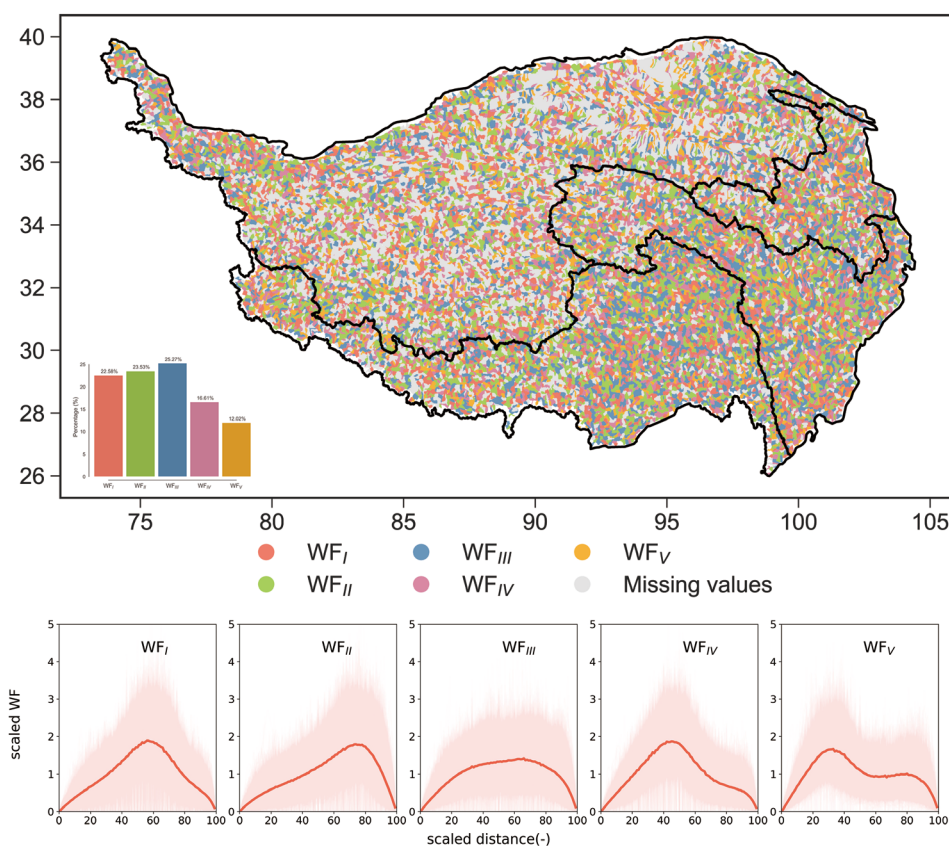
226 The width function of a catchment is a comprehensive curve reflecting the effects of landform on hydrological behavior
 227 and is used to develop the instantaneous unit hydrograph for catchments across the TP. In TPHGD, normalized width functions
 228 of 13,456 out of the 18,440 catchments are presented since it is less meaningful to derive the width function of a catchment
 229 with a relatively smaller area. The normalized width functions of the 13,456 catchments across the TP are grouped into five
 230 types by using the K-means unsupervised clustering approach and the Gap Statistic method.

231 Shapes of the five types of width functions are shown in Figure 6. The first two types of width function both have a
 232 notable peak value in the curve (i.e., area proportion against distance to catchment outlet). However, the WF_I is peak-centered
 233 while WF_{II} is peak-skewed. The shape of catchments characterized by these two types of width functions is typically elongated,
 234 with tributaries predominantly located in the upstream areas, resulting in relatively lengthy routing pathways. The third type
 235 of the width function (WF_{III}) is largely uniform-like without notable peaks. This width function type is often observed in
 236 catchments with larger overall areas or with a relatively consistent density of river networks extending from upstream to
 237 downstream. The fourth (WF_{IV}) and fifth (WF_V) types of width function are with dual peaks. The main difference between
 238 them is that the first peak in WF_{IV} is dominant, while the two peaks in WF_V are much closer values. Catchments with WF_{IV} or



239 WF_V approximately are parallel river systems, having more tributaries converging separately to catchment outlets than other
240 catchments.

241 For the 13,456 catchments across TP, the proportion of catchments with a specific width function type are 22.58% (WF_I),
242 23.53% (WF_{II}), 25.27% (WF_{III}), 16.61% (WF_{IV}) and 12.02% (WF_V) respectively. As shown in Figure 6, however, there is no
243 clear spatial pattern of the width function across the TP. The spatial distribution characteristics of the width function are
244 relatively random, and the obvious spatial aggregation characteristics of different classification width functions cannot be
245 found in our dataset.



246

247 **Figure 6 Typical width functions (bottom) and their spatial distribution across the Tibetan Plateau (top). At the bottom, the pink**
248 **background indicates ranges of width function from catchments subset of that type, while the red curve represents the median of**
249 **the corresponding catchment subset.**

250 4.3 WFIUH of catchments across the Tibetan Plateau

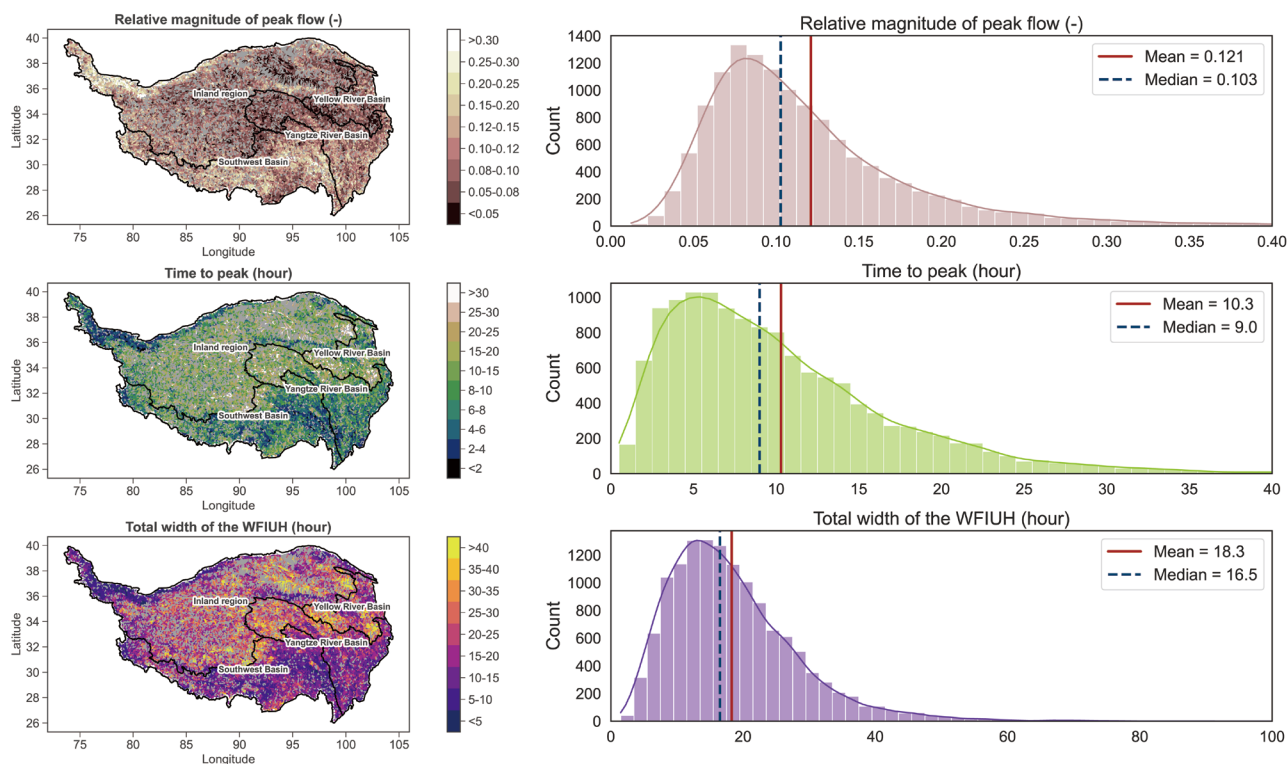
251 Based on the catchments' width function, instantaneous unit hydrographs for each of the 13,456 catchments across the
252 TP are derived and presented in the TPHGD dataset, together with flow velocity estimated by Manning's approach for each
253 grid cell. The time interval of the derived WFIUH is 30 minutes. There are some catchments located in the eastern Continental
254 basin whose WFIUH cannot be extracted due to large irrigation areas and canals. Herein, characteristics of the WFIUH



255 indicated by peak flow magnitude (Q_p), time to peak (T_p) and concentration time (T_c , i.e., width of time base in WFIUH) for
256 catchments across the TP are investigated. Their relationships with the 18 geomorphic metrics are also examined. The box plot
257 of the relative magnitude of peak flow, time to peak, and the total width of the WFIUH and the spatial pattern of the three
258 variables is demonstrated in Figure 7. This information can reveal the distribution features of the WFIUH of 13456 catchments
259 in the Tibetan Plateau, which may be valuable for flood risk decision-making and management in this region.

260 As shown in Figure 7, the relative magnitude of peak flow for most catchments ranges from 0.05 to 0.15, with mean and
261 median are 0.121 and 0.103 respectively. The smaller relative magnitude of the peak flow value represents a more uniform
262 hydrograph distribution and a less obvious peak. The higher the Q_p , the more susceptible the catchment is to flash floods.
263 Catchments with a higher Q_p are found in the northwest or north edge of the Inland Region (IR). Catchments in central IR
264 have relatively lower Q_p due to their smaller slopes. Catchments in the upper Yellow River Basin (YLRB) and Yangtze River
265 Basin (YZRB) have correspondingly smaller Q_p than catchments in lower YLRB and YZRB. Catchments in the Southwest
266 Basin (SWB) have the highest Q_p as compared to catchments in the other three regions. Particularly, in Nu River, Jinsha River,
267 Lancang River, and the Palong Zangbo area, Q_p can reach 0.2 and above, which explains well the high flood risks in those
268 regions. In the middle and lower reaches of the Yarlung Zangbo River and the Shiquan River area, the relative magnitude of
269 peak flow is also higher than that of the whole Tibetan Plateau.

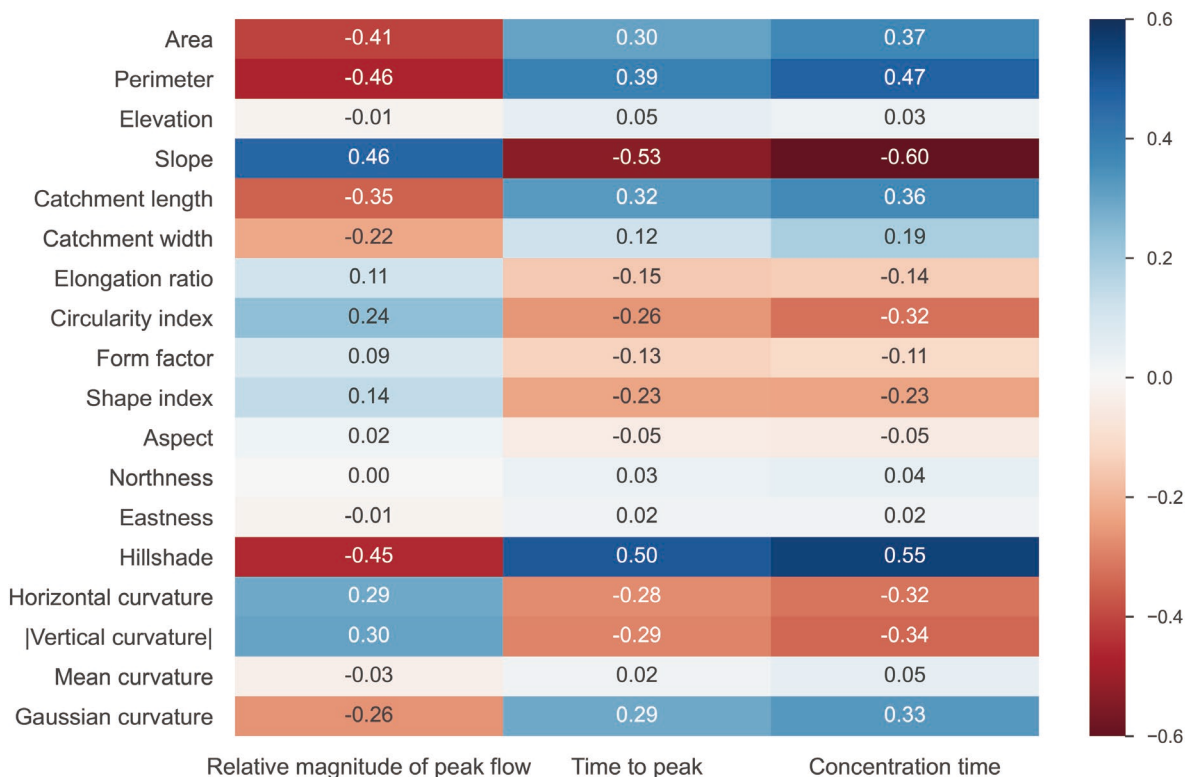
270 The time to peak time in most catchments mainly ranges from 2h to 15 h, with mean and median T_p around 10.3h and
271 9.0h respectively. The spatial distribution of T_p across the Tibetan Plateau is similar to that of Q_p , suggesting the shorter the
272 T_p , the higher the Q_p is. Catchment concentration time however varies from 10h-35h, with mean and median T_c around 18.3h
273 and 16.5h respectively. Catchments with longer T_c are found in the central TP and YLRB. Catchments in the northwest IR,
274 middle and lower reaches of the Yarlung Zangbo River, Palong Zangbo River and the Nu-Jinsha-Lancang basins all have
275 relatively short T_c (<20h). For those regions with high Q_p , short T_p and T_c , it is mainly because the catchments there tend to
276 elongate and with a pinnate river network, higher slope and lower roughness.



277

278 **Figure 7 Distribution of WFIUH characteristics across the Tibetan Plateau. Left: spatial distribution; right: statistical distribution**
279 **represented by histogram.**

280 Figure 8 further shows the relationships of Q_p , T_p and T_c against the 18 hydrogeomorphic metrics in our TPHGD dataset.
281 It is found that Q_p is positively related to slope, horizontal curvature and absolute vertical curvature. Q_p is negatively related
282 to catchment area, perimeter, length and circularity. The relationships of T_p against the hydrogeomorphic metrics are similar
283 to those of Q_p but in an opposite direction. This suggests that a catchment with a larger, more circular shape may exhibit a
284 more gradual rising limb in its hydrograph. T_c has a strong negative correlation with catchment slope as a steeper land surface
285 can result in faster flow hence shortening the travelling time of water flow. Unsurprisingly, T_c is positively related to catchment
286 size defined by area, perimeter and length.



287

288 **Figure 8 Correlations between WFIUH characteristics against 18 hydrogeomorphic metrics**

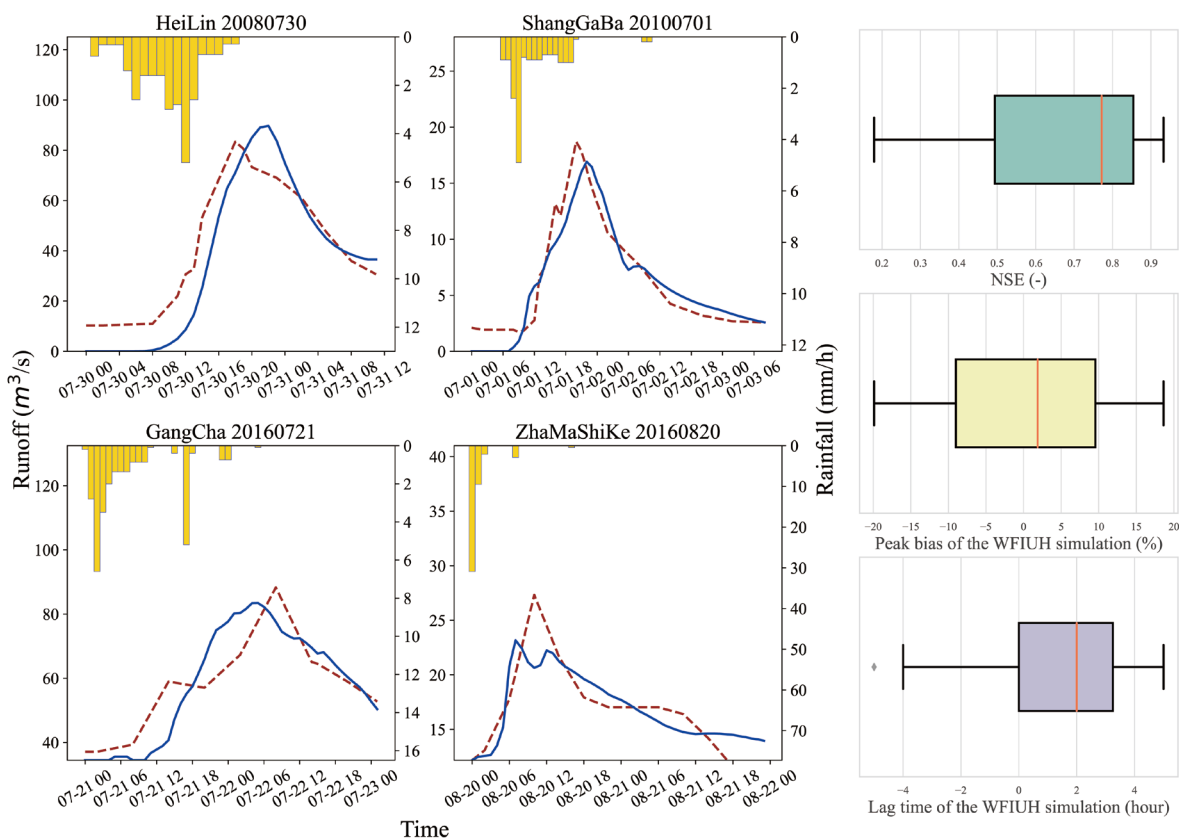
289 **4.4 Validity and uncertainty of derived WFIUH**

290 The derived WFIUH in our TPHGD dataset is expected to represent the hydrological response function in a catchment,
 291 particularly contributing to generating a hydrograph of ungauged catchments in the Tibetan Plateau. To examine the validity,
 292 we have incorporated the derived WFIUH into a conceptual hydrological model GR4H (Perrin et al., 2003). The GR4H is a
 293 model with four parameters running at an hourly time step. The fourth parameter of GR4H (x4) represents the time base of a
 294 hypothetical unit hydrograph. In this study, the hypothetical unit hydrograph is replaced by our derived WFIUH, and the
 295 parameter x4 is then removed. The model was tested at four gauged catchments in the Tibetan Plateau for 48 flash flood events
 296 from 2008 to 2016. The required inputs of the model (rainfall and potential evapotranspiration) and the observed hourly
 297 streamflow data are obtained from China's Annual Hydrological Report.

298 Overall, the model performs well for most of the flash flood events as evaluated by NSE (Nash and Sutcliffe, 1970), bias
 299 in peak flow (BS_{qp}) and bias in time to peak (BS_{tp}) respectively (Figure 9). The simulated hydrograph is compared to the
 300 observed one for selected catchments and is shown in Figure 9 as well. As shown in Figure 9, the median NSE of the 48 flash
 301 events is around 0.67, for more than 50% of the 48 flash flood events with an absolute value of BS_{qp} lower than 10% and an
 302 absolute value of BS_{tp} lower than 3h. Peak flows of 26 flood events are underestimated while that of the other 22 events are



303 overestimated, suggesting no systematic tendency in the modelling. The time to peak (T_p) of about two-thirds of simulated
 304 flood events lags behind the observed one, indicating uncertainties in the simulations.



305
 306 **Figure 9** Performance of hydrological modeling by incorporating WFIUH into GR4H model. Left: comparison between simulated
 307 and observed hydrograph for flash events at different catchments (red-dashed curve is observed, blue-solid curve is simulated);
 308 **Right**, summary of overall model performance for 48 simulated flash flood events.

309 Uncertainties of the simulation can not only be due to the uncertainties in the derived WFIUH but also due to uncertainties
 310 in model structure, model inputs and model parameters. In terms of WFIUH, its validity could be affected by the spatial
 311 resolution and sources of DEM and the effectiveness of the method in estimating flow velocity. In this study, the DEM dataset
 312 from SRTM is used, which has with spatial resolution of 90m. We find it challenging to derive WFIUH for catchments with
 313 relatively small areas and with highly complicated topography by using the DEM from SRTM. Hence, DEM with higher
 314 spatial resolution can be conducive to improving the derivation of WFIUH for those catchments. It is worth noting that the
 315 uncertainties in WFIUH could be considerably affected by the estimate of flow velocity. In this study, Manning’s approach is
 316 used to calculate flow velocity at each grid cell and then works with the catchment’s width function to derive the WFIUH.
 317 Other approaches such as the Darcy–Weisbach formula (Katz et al., 1995), the Soil Conservation Service (SCS) formula (Haan
 318 et al., 1994), and the Maidment et al. (1996) uniform flow equation may result in a different estimate of flow velocity and
 319 hence the subsequent WFIUH. In addition, the roughness coefficient in Manning’s approach assigned for each grid cell is



320 affected by the accuracy of the land cover map, leading to uncertainties in the estimated flow velocity. It has been reported
321 that a higher deviation in the roughness coefficient could result in a higher deviation of the hydrograph peaks (Kalyanapu et
322 al., 2009). Thus, a detailed evaluation of Manning’s roughness in different land cover types using remote sensing skills is
323 needed to reduce the uncertainties (Mtamba et al., 2015; Sadeh et al., 2018). For further exploration of the uncertainties in the
324 future, therefore in this version of the dataset, we provide also the width function for each catchment, which facilitates deriving
325 WFIUH given different estimates of flow velocity.

326 5 Data and code availability

327 Our TPHGD dataset provides 18 hydrogeomorphic metrics for 18440 catchments across the Tibetan Plateau, together
328 with width function and WFIUH of 13456 out of the 18440 catchments. Table 2 lists the structure of the dataset and the formats
329 of the files there. The 18 metrics of all catchments are presented in an Excel file. The catchment’s width function is stored in
330 two separate CSV files, one of which represents the distance to the catchment outlet (i.e., x-axis in the WF plot) while the
331 other represents the number of cells (equivalent to counts representing y-axis in the WF plot) at a given distance to the outlet.
332 The gridded flow velocity map is presented as a tif file in Manning_velocity_map. Similar to the catchment’s WF, WFIUH
333 for each catchment is presented in two paired CSV files, WFIUH_flowtime.csv and WFIUH_cells.csv. The former provides
334 flow time at a specific distance to the catchment outlet (i.e., the x-axis in the WFIUH plot), while the latter provides the number
335 of cells (equivalent to counts and representing the y-axis in the WFIUH plot) within the corresponding distance. The dataset
336 is archived and openly accessible via the Zenodo portal: <https://doi.org/10.5281/zenodo.8280786> (Guo and Zheng, 2023).

337 The Python scripts in deriving WFIUH, curve fitting, and classification are freely available at
338 https://github.com/YuhanGuo-22/Hydro_WFIUH_Classifier_and_Curve_fitting.git (last access: 18 Oct 2023). The
339 dependency Python package (pysheds) used in deriving catchment WF is available at <https://github.com/mbartos/pysheds>.

340

341 **Table 2 Files in the TPHGD dataset**

File names	Formats	Descriptions
1-Hydro_geomorphic_attribute	.xlsx 18440× 26	Hydrogeomorphic metrics of 18440 catchments. Each row represents one catchment. Each column represents one metric (see Table 1).
2-WF_distance	.csv 13456 columns	Catchments’ width function: distance to outlet (WF’s x-axis). The first row is the catchment ID. Each column represents the distance to the catchment outlet for a catchment.
2-WF_cells.csv	.csv 13456 columns	Catchments’ width function: cells/area (WF’s y-axis). The first row is the catchment ID. Each column represents cells between a specific distance and an outlet for a catchment.
3-Manning_velocity_map	.tif (90m resolution)	Gridded flow velocity was calculated by Manning’s approach. The value of each grid represents the mean velocity along the shortest flow path to the outlet.



4-WFIUH_flowTime.csv	.csv 13456 columns	Catchments' WFIUH: flow time to the outlet (WFIUH's x-axis). The first row is the catchment ID. Each column represents flow time to the outlet for a catchment.
4-WFIUH_cells.csv	.csv 13456 columns	Catchments' WFIUH: cells/area to outlet corresponding to a specific flow time (WFIUH's y-axis). The first row is the catchment ID. Each column represents the number of cells with a specific flow time to the outlet of a catchment.

342

343 6 Conclusions

344 The Tibetan Plateau provides an ideal setting for investigating the interactions between hydrological and geomorphic
345 processes in a largely pristine natural environment, minimally impacted by human activities. The hydrological behaviours of
346 catchments across the Tibetan Plateau however remain largely unknown due to its challenging physical conditions and data
347 limitations. This study presents the inaugural version of a hydrogeomorphic dataset encompassing 18,440 catchments across
348 the region. The dataset comprises 18 hydrogeomorphic metrics, particularly along with the width function and width function-
349 based instantaneous unit hydrograph of each catchment. It can contribute to advancing our understanding of catchment
350 hydrological behaviors in the Tibetan Plateau and hence improving water resources management and disaster mitigation in the
351 region and its downstream.

352 According to the dataset provided, it is found that catchments with higher elevation are in the western and central parts
353 of the TP, while catchments in the western and southeast TP are steeper than other catchments in the TP. Catchments in central
354 TP are more elongated with the pinnate river network, and catchments in western and eastern TP are less elongated and more
355 fan-shaped. A power relationship (i.e., Hack's law) exists between catchments' area and length. We also find that the peak
356 flow of WFIUH is positively related to slope and curvature but negatively related to catchment area, perimeter, length and
357 circularity. The relationships of time-to-peak against the hydrogeomorphic metrics are similar to those of peak flow but in an
358 opposite direction. These results suggest that a catchment with a larger size and with a more circular shape may exhibit a
359 more gradual rising limb in its hydrograph. Catchment concentration time shows a positive relationship with catchment size
360 but a strong negative correlation with catchment slope as a steeper land surface can result in faster flow hence shortening the
361 travelling time of water flow. The validity of the derived WFIUH has been confirmed by its successful integration into an
362 hourly hydrological model for simulating flash flood events. Uncertainties in the simulation may arise from factors such as
363 model structure, model inputs, model parameterization, and the derived WFIUH. Particularly, uncertainties in the WFIUH can
364 be attributed to the resolution of DEM and the methods employed for calculating flow velocity. These aspects warrant further
365 exploration in future research endeavors.

366

367 **Author contributions.**



368 HZ, YS, YY and YG conceived the research. YG and HZ developed the approaches and datasets. YY and YS checked the
369 results. YG and HZ wrote the original draft. YY, YS and CW revised the draft.

370

371 **Competing interests.**

372 The contact author has declared that none of the authors has any competing interests.

373 **References**

- 374 Babar, M.: Hydrogeomorphology: fundamentals, applications and techniques, 2005.
375 Bhaskar, N. R., Parida, B. P., and Nayak, A. K.: Flood estimation for ungauged catchments using the GIUH, Journal of water resources
376 planning management, 123, 228-238, 1997.
377 Botter, G. and Rinaldo, A.: Scale effect on geomorphologic and kinematic dispersion, Water Resources Research, 39, 2003.
378 Esper Angillieri, M. Y.: Morphometric analysis of Colangüil river basin and flash flood hazard, San Juan, Argentina, Environmental geology,
379 55, 107-111, 2008.
380 Florinsky, I.: Digital terrain analysis in soil science and geology, Academic Press 2016.
381 Franchini, M. and O'Connell, P. E.: An analysis of the dynamic component of the geomorphologic instantaneous unit hydrograph, Journal
382 of Hydrology, 175, 407-428, 1996.
383 Franchini, M. and O'Connell, P. E.: An analysis of the dynamic component of the geomorphologic instantaneous unit hydrograph, Journal of
384 Hydrology, 175, 407-428, 10.1016/S0022-1694(96)80018-7, 1996.
385 Ge, J., You, Q., and Zhang, Y.: Effect of Tibetan Plateau heating on summer extreme precipitation in eastern China, Atmospheric Research,
386 218, 364-371, 2019.
387 Grimaldi, S., Petroselli, A., Alonso, G., and Nardi, F.: Flow time estimation with spatially variable hillslope velocity in ungauged basins,
388 Advances in Water Resources, 33, 1216-1223, 10.1016/j.advwatres.2010.06.003, 2010.
389 Guo, Y. and Zheng, H.: Hydro-geomorphic unit hydrograph dataset of catchments across the Tibetan Plateau, Zenodo [data set],
390 <https://doi.org/10.5281/zenodo.8280786>, 2023.
391 Gupta, V. K. and Waymire, E.: On the formulation of an analytical approach to hydrologic response and similarity at the basin scale, Journal
392 of Hydrology, 65, 95-123, 1983.
393 Gupta, V. K., Waymire, E., and Wang, C.: A representation of an instantaneous unit hydrograph from geomorphology, Water resources
394 research, 16, 855-862, 1980.
395 Haan, C. T., Barfield, B. J., and Hayes, J. C.: Design hydrology and sedimentology for small catchments, Elsevier 1994.
396 Horton, R. E.: Erosional development of streams and their drainage basins-Hydrophysical approach to quantitative morphology, Bull. G. S.
397 A, 56, 1945.
398 Jain, S., Singh, R., and Seth, S.: Design flood estimation using GIS supported GIUH Approach, Water resources management, 14, 369-376,
399 2000.
400 Jensen, S. K.: Applications of hydrologic information automatically extracted from digital elevation models, Hydrol. Process., 5, 31-44,
401 1991.
402 Kalyanapu, A. J., Burian, S. J., and McPherson, T. N.: Effect of land use-based surface roughness on hydrologic model output, Journal of
403 Spatial Hydrology, 9, 2009.
404 Kang, S., Xu, Y., You, Q., Flügel, W.-A., Pepin, N., and Yao, T.: Review of climate and cryospheric change in the Tibetan Plateau,
405 Environmental research letters, 5, 015101, 2010.
406 Katz, D. M., Watts, F. J., and Burroughs, E. R.: Effects of surface roughness and rainfall impact on overland flow, Journal of Hydraulic
407 Engineering, 121, 546-553, 1995.
408 Kirkby, M.: Tests of the random network model, and its application to basin hydrology, Earth Surface Processes, 1, 197-212, 1976.
409 Kirshen, D. M. and Bras, R. L.: The linear channel and its effect on the geomorphologic IUH, Journal of Hydrology, 65, 175-208, 1983.
410 Koenderink, J. J. and Van Doorn, A. J.: Surface shape and curvature scales, Image vision computing, 10, 557-564, 1992.
411 Kumar, R., Chatterjee, C., Singh, R., Lohani, A., and Kumar, S.: Runoff estimation for an ungauged catchment using geomorphological
412 instantaneous unit hydrograph (GIUH) models, Hydrological Processes: An International Journal, 21, 1829-1840, 2007.
413 Lehner, B., Verdin, K., and Jarvis, A.: New Global Hydrography Derived From Spaceborne Elevation Data, Eos, Transactions American
414 Geophysical Union, 89, 93, 10.1029/2008eo100001, 2008.
415 Li, X., Long, D., Scanlon, B. R., Mann, M. E., Li, X., Tian, F., Sun, Z., and Wang, G.: Climate change threatens terrestrial water storage
416 over the Tibetan Plateau, Nature Climate Change, 12, 801-807, 10.1038/s41558-022-01443-0, 2022.
417 Lindersson, S., Brandimarte, L., Mård, J., and Di Baldassarre, G.: Global riverine flood risk—how do hydrogeomorphic floodplain maps
418 compare to flood hazard maps?, Natural hazards earth system sciences, 21, 2921-2948, 2021.



- 419 Maidment, D., Olivera, F., Calver, A., Eatherall, A., and Fraczek, W.: Unit hydrograph derived from a spatially distributed velocity field,
420 *Hydrol. Process.*, 10, 831-844, 1996.
- 421 Mesa, O. J. and Mifflin, E. R.: On the relative role of hillslope and network geometry in hydrologic response, in: *Scale problems in hydrology*,
422 Springer, 1-17, 1986.
- 423 Mölg, T., Maussion, F., and Scherer, D.: Mid-latitude westerlies as a driver of glacier variability in monsoonal High Asia, *Nature Climate*
424 *Change*, 4, 68-73, 10.1038/nclimate2055, 2014.
- 425 Moussa, R.: What controls the width function shape, and can it be used for channel network comparison and regionalization?, *Water*
426 *Resources Research*, 44, 19, 10.1029/2007wr006118, 2008.
- 427 Mtamba, J., Van Der Velde, R., Ndomba, P., Zoltán, V., and Mtaló, F.: Use of Radarsat-2 and Landsat TM Images for Spatial
428 Parameterization of Manning's Roughness Coefficient in Hydraulic Modeling, *Remote Sensing*, 7, 836-864, 10.3390/rs70100836, 2015.
- 429 NADEN, P. S.: Spatial variability in flood estimation for large catchments: the exploitation of channel network structure, *Hydrological*
430 *Sciences Journal*, 37, 53-71, 1992.
- 431 Nash, J. E. and Sutcliffe, J. V.: River flow forecasting through conceptual models part I—A discussion of principles, *Journal of Hydrology*,
432 10, 282-290, 1970.
- 433 Nasri, S., Cudennec, C., Albergel, J., and Berndtsson, R.: Use of a geomorphological transfer function to model design floods in small
434 hillside catchments in semiarid Tunisia, *Journal of hydrology*, 287, 197-213, 2004.
- 435 Nowicka, B. and Soczynska, U.: Application of GIUH and dimensionless hydrograph models in ungauged basins, *FRIENDS in Hydrology*,
436 187, 197-203, 1989.
- 437 Passalacqua, P., Tarolli, P., and Foufoula-Georgiou, E.: Testing space-scale methodologies for automatic geomorphic feature extraction from
438 lidar in a complex mountainous landscape, *Water resources research*, 46, 2010.
- 439 Peng Gong, Han Liu, Meinan Zhang, Li, C., Wang, J., and Huang, H.: Stable classification with limited sample: Transferring a 30-m
440 resolution sample set collected in 2015 to mapping 10-m resolution global land cover in 2017, *Sci. Bull.*, 64, 370-373, 2019.
- 441 Perrin, C., Michel, C., and Andréassian, V.: Improvement of a parsimonious model for streamflow simulation, *Journal of hydrology*, 279,
442 275-289, 2003.
- 443 Rigon, R., Rodriguez-Iturbe, I., Maritan, A., Giacometti, A., Tarboton, D. G., and Rinaldo, A.: On Hack's Law, *Water Resources Research*,
444 32, 3367-3374, 10.1029/96wr02397, 1996.
- 445 Rinaldo, A., Marani, A., and Rigon, R.: Geomorphological dispersion, *Water Resources Research*, 27, 513-525, 1991.
- 446 Rinaldo, A., Vogel, G. K., Rigon, R., and Rodriguez-Iturbe, I.: Can one gauge the shape of a basin, *Water Resources Research*, 31, 1119-
447 1127, 10.1029/94wr03290, 1995.
- 448 Rodriguez-Iturbe, I. and Valdes, J. B.: The geomorphologic structure of hydrologic response, *Water resources research*, 15, 1409-1420, 1979.
- 449 Rodriguez-Iturbe, I. and Valdes, J. B.: The geomorphologic structure of hydrologic response, *Water resources research*, 15, 1409-1420, 1979.
- 450 Saco, P. M. and Kumar, P.: Kinematic dispersion effects of hillslope velocities, *Water Resources Research*, 40, n/a-n/a,
451 10.1029/2003wr002024, 2004.
- 452 Sadeh, Y., Cohen, H., Maman, S., and Blumberg, D.: Evaluation of Manning's n Roughness Coefficient in Arid Environments by Using
453 SAR Backscatter, *Remote Sensing*, 10, 1505, 10.3390/rs10101505, 2018.
- 454 Safanelli, J., Poppiel, R., Ruiz, L., Bonfatti, B., Mello, F., Rizzo, R., and Demattê, J.: Terrain Analysis in Google Earth Engine: A Method
455 Adapted for High-Performance Global-Scale Analysis, *ISPRS International Journal of Geo-Information*, 9, 400, 10.3390/ijgi9060400,
456 2020.
- 457 Sassolas-Serrayet, T., Cattin, R., and Ferry, M.: The shape of watersheds, *Nature Communications*, 9, 10.1038/s41467-018-06210-4, 2018.
- 458 Scheidegger, A. E.: Hydrogeomorphology, *Journal of Hydrology*, 20, 193-215, 1973.
- 459 Sidle, R. C. and Onda, Y.: Hydrogeomorphology: overview of an emerging science, *Hydrol. Process.*, 18, 597-602, 2004.
- 460 Singh, P., Mishra, S., and Jain, M.: A review of the synthetic unit hydrograph: from the empirical UH to advanced geomorphological methods,
461 *Hydrological Sciences Journal*, 59, 239-261, 2014.
- 462 Strahler, A. N.: Quantitative analysis of watershed geomorphology, *Eos, Transactions American Geophysical Union*, 38, 913-920, 1957.
- 463 Troutman, B. M. and Karlinger, M. R.: Unit hydrograph approximations assuming linear flow through topologically random channel
464 networks, *Water Resources Research*, 21, 743-754, 10.1029/wr021i005p00743, 1985.
- 465 Yang, L., Ma, J., Wang, X., and Tian, F.: Hydroclimatology and Hydrometeorology of Flooding Over the Eastern Tibetan Plateau, *Journal*
466 *of Geophysical Research: Atmospheres*, 127, e2022JD037097, 2022.
- 467 Yao, T., Thompson, L., Yang, W., Yu, W., Gao, Y., Guo, X., Yang, X., Duan, K., Zhao, H., Xu, B., Pu, J., Lu, A., Xiang, Y., Kattel, D. B.,
468 and Joswiak, D.: Different glacier status with atmospheric circulations in Tibetan Plateau and surroundings, *Nature Climate Change*, 2,
469 663-667, 10.1038/nclimate1580, 2012.
- 470 Yao, T., Bolch, T., Chen, D., Gao, J., Immerzeel, W., Piao, S., Su, F., Thompson, L., Wada, Y., Wang, L., Wang, T., Wu, G., Xu, B., Yang,
471 W., Zhang, G., and Zhao, P.: The imbalance of the Asian water tower, *Nature Reviews Earth & Environment*, 10.1038/s43017-022-
472 00299-4, 2022.
- 473